

Probing neutron-star matter in the lab: connecting binary mergers to heavy-ion collisions

Elias R. Most,^{1,2,3} Anton Motornenko,^{4,5} Jan Steinheimer,⁵ Veronica Dexheimer,⁶
Matthias Hanauske,^{4,5} Luciano Rezzolla,^{4,5,7} and Horst Stoecker^{4,5,8}

¹Princeton Center for Theoretical Science, Princeton University, Princeton, NJ 08544, USA

²Princeton Gravity Initiative, Princeton University, Princeton, NJ 08544, USA

³School of Natural Sciences, Institute for Advanced Study, Princeton, NJ 08540, USA

⁴Institut für Theoretische Physik, Goethe Universität, D-60438 Frankfurt am Main, Germany

⁵Frankfurt Institute for Advanced Studies, Giersch Science Center, D-60438 Frankfurt am Main, Germany

⁶Department of Physics, Kent State University, Kent, OH 44243, USA

⁷School of Mathematics, Trinity College, Dublin 2, Ireland

⁸GSI Helmholtzzentrum für Schwerionenforschung GmbH, D-64291 Darmstadt, Germany

(Dated: February 1, 2022)

As a way to find analogies and differences in the dynamics of hot and dense matter under extreme conditions, we present the first self-consistent relativistic-hydrodynamic calculations of both neutron-star mergers and low-energy heavy-ion collisions employing the same equation of state. By a direct comparison of the evolution of quantities such as temperature, entropy, and density, we show that neutron-star collision regimes can be probed directly at GSI beam energies. We provide concrete evidence that the physical conditions reached in binary neutron-star mergers can be studied in present and future laboratory experiments, thus bridging 18 orders of magnitude in length scale, from microscopic ion collisions to macroscopic astrophysical compact objects.

Introduction. Quantum Chromodynamics (QCD), the theory of strong interactions, predicts that high-energy matter formed in both, binary neutron-star (BNS) mergers and heavy-ion collisions (HICs), consists of the same particles that obey the same interactions. The recent detection of gravitational waves from BNSs [1, 2] naturally raises the question whether it is possible to produce and study the same state of hot, compressed matter in both BNS mergers and HICs. In particular, whether a transition from hadron to quark matter can occur at or after the merger [3–9]. To date, the former question has been addressed only rather qualitatively. Interestingly, early simulations have shown a possible overlap in temperature and (baryon number) density [7, 10], as well as the geometry of the system [11]. Going beyond all of these works, we present the first simulations of low-energy HICs and low-mass BNSs using the same realistic and relativistic chiral equation of state (EOS) to describe hot dense matter. This allows to uniquely identify the differences and similarities in compression, temperature, entropy and isospin, as well as comparing carefully the dynamical evolution of the geometry of the two systems. In this way, we can map specific microscopic initial conditions in the laboratory to macroscopic mergers consistent with previous gravitational-wave events [1, 2, 12], and obtain information on the properties of compact stars, such as the maximum mass [13–16], or typical radii and tidal deformabilities [17–33].

Methods. Here, a brief outline of the methods employed in this paper is presented, the most crucial one being the description of nuclear matter. A meaningful comparison between the regimes probed in BNS mergers and HICs requires a realistic, consistent model for the EOS that is valid across a very large portion of the QCD phase diagram. Such a description should be consistent with constraints from cold compact stars (e.g., [34–41]), properties of symmetric nuclear matter around nuclear saturation density n_{sat} [42–55], as well

as large temperature QCD constraints at vanishing and finite density. In the latter case, a consistent description for chiral-symmetry restoration and quark deconfinement must be included to reproduce data from lattice QCD [56–58], perturbative QCD [59, 60], and high-energy collider experiments [61]. Addressing all of the above, we make use of the Chiral Mean Field (CMF) model, which is based on the three-flavor chiral Lagrangian for hadronic matter first introduced in [62] and extended to describe neutron stars in [63]. Our version of the CMF model [64] incorporates a full list of QCD degrees of freedom: an interacting baryon octet with respective negative parity partners, a full PDG (Particle Data Group [65]) list of baryons and mesons, leptons, as well as deconfined quark degrees of freedom [66]. The change from hadronic to deconfined degrees of freedom takes place self-consistently through an excluded-volume prescription [67], which suppresses hadrons at high energies, and a PNJL (Polyakov-loop-extended Nambu Jona-Lasinio) description of quarks and gluons [68, 69], which suppresses the deconfined quark degrees of freedom at moderate energies.

As a result, a crossover transition for deconfinement occurs at both, finite and zero temperature, providing a good description for hadrons in medium, nuclei, nuclear matter and neutron-stars [64]. This approach allows to calculate the EOS of nuclear matter created in both, HICs, as well as BNSs, in one thermodynamically consistent chiral relativistic approach, without introducing new parameters and allowing for a direct, meaningful comparison between these two seemingly different microscopic and macroscopic nuclear-matter systems.

The other critical component of our study is the perfect-fluid hydrodynamic description of both BNS mergers and HICs. We evolve in time the equations of relativistic hydrodynamics on a 3-dimensional grid, but employ different codes adapted to each system. In the case of HICs, this is done with the Frankfurt SHASTA code [70, 71], using a uniform grid

spacing $\Delta x = 0.2$ fm and timestep $\Delta t = 0.08$ fm/ c . It was shown that the HICs system dynamics and entropy production as calculated with the hydrodynamical approach are quite similar to the complementary predictions of non-equilibrium transport models [72, 73]. We are interested in simulating low-energy nuclear collisions - hence, our initial state consists of two drops of cold $T = 0$ nuclear matter, colliding head-on, with Lorentz-contracted Woods-Saxon density distributions, propagating towards each other with relativistic speed in the center-of-mass frame of the collision. For each energy, a near central collision of two gold nuclei (Au) is computed, at fixed “impact parameter” $b = 2$ fm (i.e., b is the offset of the centers of the two nuclei along the transverse x -axis), at lab energies of $E_{\text{lab}} = 450$ and 600 A MeV per nucleon. These energies are presently available for experiments of the HADES detector set-up at GSI [11].

For our BNS simulations, in addition to the equations of general-relativistic hydrodynamics [74], we need to solve the Einstein equations in the conformal Z4 formulation [75–78]. The full set of equations is evolved using the Frankfurt/IllinoisGRMHD (FIL) code [79, 80], which operates on top of the Einstein Toolkit infrastructure [81]. Making use of nested box-in-box mesh refinement [82], our simulations use 7 levels of refinement with the highest resolution of 250 m and outer box size of 1500 km. The initial conditions [83] for our simulations are two equal-mass nonspinning binaries with total masses of 2.6 and $2.8 M_{\odot}$ consistent with GW170817-like events [1]. It is important to stress that despite the use of perfect-fluid hydrodynamics and, hence, the absence of physical viscosity (see e.g., [84–87] for formulations including viscosity), our codes are fully able to capture entropy production in the compressional regime of the flow by means of local Rankine-Hugoniot shock junction conditions [74]. In the case of FIL, this is achieved by locally solving the set of Riemann problems approximately using the HLLC algorithm [88]. In the case of SHASTA, this is handled by a flux-corrected diffusion algorithm that has been thoroughly vetted [70] and compared against HLLC solvers [71].

Results and Discussion. For both, the macroscopic and the microscopic events, we have performed analogous simulations using the same description of nuclear matter, which – as discussed – is valid across the entire QCD phase diagram. Hence, despite a difference in lengthscales of 18 orders of magnitude, it is possible to perform a meaningful comparison of the first impact of the two stars and two gold ions. In the following, we will summarize the basic evolution of the two colliding systems.

For a HIC, the two gold nuclei approach each other head-on along the z -direction, with relative velocities $v \gtrsim 0.5c$ and only a small offset along the transverse x -axis, called the impact parameter b . This produces dense hot matter with the longest lifetime and highest compression at given beam energy. Once the two nuclei make contact, the cold nuclear matter in the center is rapidly heated by shock compression. During this incident stage, entropy is generated and the maximum

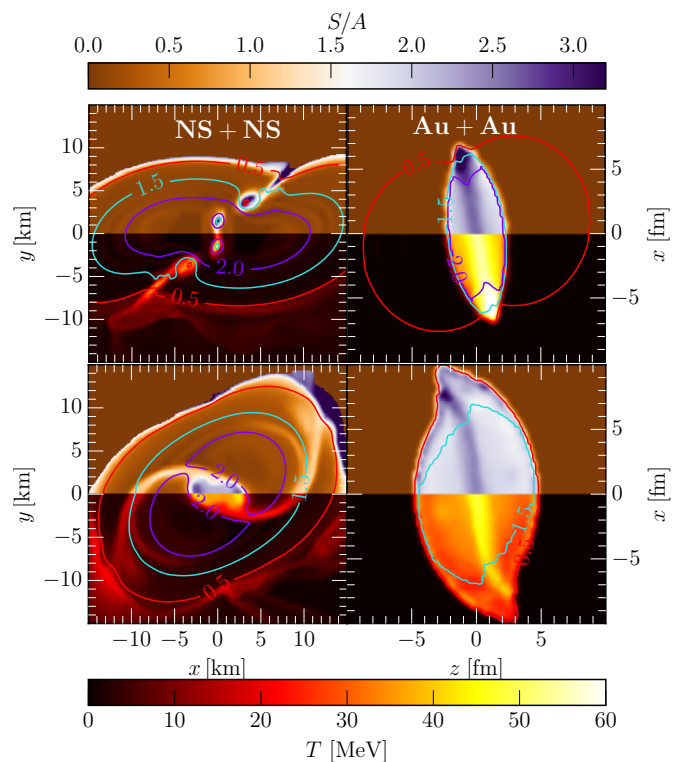


FIG. 1. Distributions of entropy per baryon S/A (top colormaps) and temperature T (bottom colormaps) for a BNS merger (NS+NS) with total mass $M_{\text{tot}} = 2.8 M_{\odot}$ (left panels) and a Au + Au HIC at $E_{\text{lab}} = 450$ MeV (right panels). Colored lines mark density contours in units of n_{sat} . The snapshots in different rows refer to $t = -2, 3$ ms after merger for the BNS, respectively, and to $t = \pm 5$ fm/ c before and after the full overlap for the HIC.

compression is reached [72, 89]. Once both incoming nuclei are compressed in a single fireball, matter starts to rapidly expand along an isentropic trajectory until the freeze-out surface, when it dilutes so much that the hydrodynamic picture is no longer valid. In our simulations, this corresponds to cells at roughly $n \sim \frac{1}{2}n_{\text{sat}} \approx 2.6 \times 10^{14}$ g cm $^{-3}$. In the case of BNSs, the two stars are initially on a quasi-circular orbit, but the emission of gravitational waves, carrying away orbital energy and angular momentum, does ultimately cause the two stars to collide (see, e.g., [90] for a review). Differently from a HIC, the collision will not be head-on. Instead, tidal forces will deform the neutron stars prior to merger, with small-scale turbulence induced in the shearing interface between the two stars (see, e.g., [91]). During the merger, the two stars are compressed to a few times n_{sat} and heated considerably, leading to supersonic velocities and the formation of a shock. This causes a steep increase in temperature and a local production of entropy, as it happens in a HIC.

The differences in the early-time dynamics between BNS mergers and HICs are shown in the top row of Fig. 1, where we report the temperature (lower colormap), the entropy per baryon (upper colormap), and the density (isocontours) for

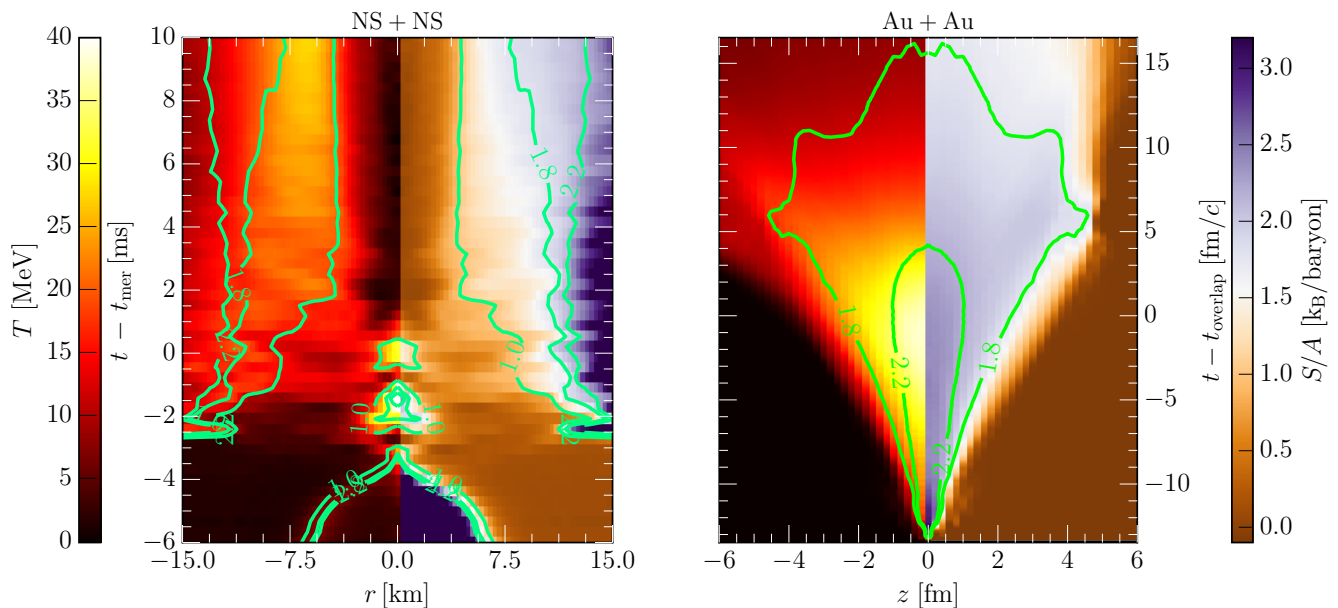


FIG. 2. Spacetime diagrams for the evolution of the temperature and entropy relative to the same BNS merger (left panel) and HIC (right panel) presented in Fig. 1. The green contours correspond to lines of constant entropy per baryon S/A ; only regions with density above freeze-out, $n > \frac{1}{2} n_{\text{sat}}$, are shown for the HIC.

a BNS collision (left panel) and a Au + Au collision (right panel). Note in the bottom row that the entropy production in BNS mergers is limited to a narrow spatial range at the interface of the two stars, where the densities probed are below $2 n_{\text{sat}}$. The precise structure of the merger remnant and, hence, the compression of layers, is governed by the strong gravitational fields present. Even some time into the collision, the heating and production of entropy is confined to the original collision interface. This is qualitatively different behaviour from what happens in HICs, where, in the early phase of the collision, entropy production is also confined to a very thin ellipsoid in the narrow initial overlap of the two nuclei. However, in the course of the reaction (the shock) compression causes the entire gold core ($n \gtrsim \frac{1}{2} n_{\text{sat}}$) to heat up. Another important difference is that, after the merger, most of the resulting object is gravitationally bound, while in the HIC case, the resulting remnant is an evanescent fireball of matter expanding isentropically at relativistic speeds. Finally, whereas in a BNS merger, the overall rotation of the system and the conservation of the Bernoulli constant [92] leads to a redistribution of hot parts of the fluid, which ultimately settles down in a ring-like structure [92, 93], the hot fireball produced in a HIC cools rapidly, during the fast, isentropic expansion, with the central region always being at the highest temperature.

While the systems themselves have very different post-collision/merger dynamics, the main feature concerning the generation of shock-heated and dense matter at the collision/merger interface is impressively similar (see Fig. 1). Additional similarities are found when comparing the dynamics of both systems in terms of the entropy per baryon

$S/A \simeq 2$ which is locally produced by shocks during the collision/merger.

Exploiting these analogies, we can compare the collision dynamics of the two systems by identifying the most important but distinct initial properties in the two systems which lead to the same production of entropy S/A in the collision, namely, the beam energy, in the case of HICs, and the total mass, in BNS mergers. To illustrate this behavior, we directly contrast the evolution of the entropy in the two different systems. The detailed comparison is shown in Fig. 2 in terms of $1 + 1$ spacetime diagrams. In order to reduce the dimensionality of the collisions, we restrict to the equatorial (x, y) plane for the BNS merger and average out the azimuthal dependence, so that $r := (x^2 + y^2)^{\frac{1}{2}}$. In the case of the HIC, the whole transverse dependence in the (x, y) plane is averaged out.

We start by considering the BNS merger, and use the left panel of Fig. 2 to illustrate that, before the collision, the temperatures and entropies are low. Tidal interactions during the inspiral can lead to a mild heating of the outer layers of the stars, but this is negligible as compared to the shock temperatures reached in the merger [94]. At the time of the merger, i.e., $t \simeq -3 \text{ ms}^{\dagger}$, regions of very high temperature and entropy are formed around $r \simeq 5 \text{ km}$. Note that the merger remnant undergoes a significant thermodynamical evolution. The presence of large angular momentum – the residual of the orbital

[†] The merger time is set when the gravitational-wave amplitude has its first maximum [95] a few milliseconds after the stellar surfaces have touched [96].

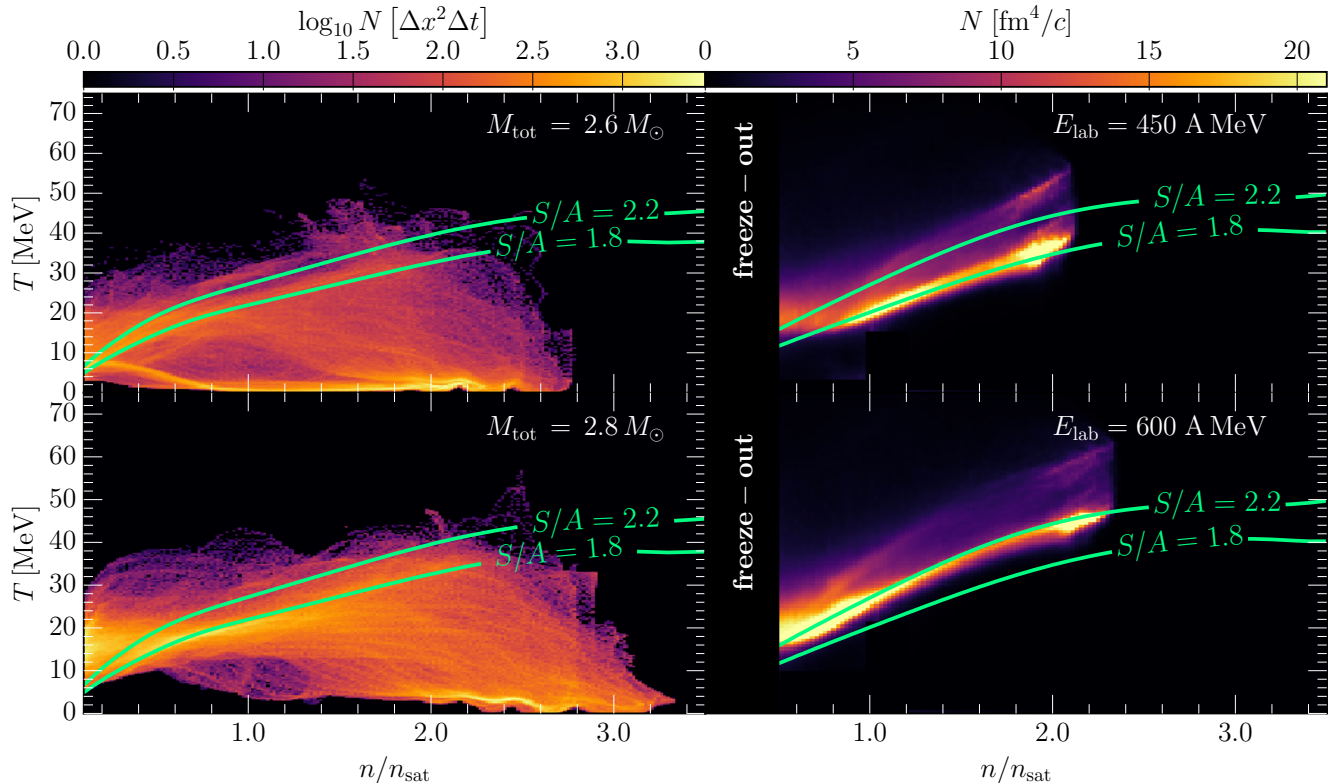


FIG. 3. Regions of the QCD phase-diagram probed by two BNS mergers with different masses (left panels) and by two HICs with different beam energies (right panels). The colorcode reports the number of cells N in the various spacetimes having a given value of temperature and density. The green lines show contours of constant entropy per baryon. Only cells with density above freeze-out, $n > \frac{1}{2} n_{\text{sat}}$, are shown for the HIC.

angular momentum, not radiated via gravitational waves – generates large shear flows despite of the fact that the two stars were initially assumed irrotational. These shear flows transport outwards the temperature and the entropy, leaving a comparatively cold and dense core (see regions with $r \lesssim 3$ km) surrounded by a much hotter ring-like structure that remains stationary in time [10] ($4.0 \lesssim r \lesssim 7$ km). The temperature and density further decrease when moving to the outer regions of the remnant ($r \gtrsim 8$ km). A similar behaviour is shown by the evolution of the entropy distribution, which exhibits a dense core with small entropy, surrounded by a hot ring with $S/A \simeq 1 - 2$.

The spacetime diagram for a HIC (right panel of Fig. 2) shows an ever increasing central-shock zone of large-entropy and high-temperature dense matter produced from the initial collision, starting from $t \simeq -15$ fm/c and up to the moment of full overlap of the two nuclei. Subsequently, the interpenetration stage of the two nuclei is over. Hence, the ellipsoid of arrested, hot, shock-heated, and compressed matter, can expand freely forwards and backwards along the collision axes at $|z| > 4$ fm. The expansion of matter is essentially isentropic, with average entropies of $S/A \approx 2.5$. Note that the averaging procedure causes a small apparent decrease of the entropy, which is only due to the averaging of asymmetries

arising from the off-center collision (see also Fig. 3).

When comparing the two panels in Fig. 2, it is important to note that there are striking analogies in the post-collision dynamics, but also that these are confined mostly to the merger phase. This is because the post-collision in a BNS is intrinsically different from that in a HIC: in the former case, strong gravitational fields lead to a remnant that is gravitationally bound and in a metastable equilibrium [91]. By contrast, the hot and dense matter produced in HICs is unbound and quickly expands into the surrounding vacuum.

The quite similar trajectories of the BNS mergers and the HICs in the QCD phase diagram may appear surprising at first sight, since they differ in chemical composition. We recall that the nuclei used in HICs consist of an almost equal number of neutrons and protons, corresponding to nearly isospin-symmetric matter, i.e., $Y_{\text{iso}} \simeq -0.1$. On the other hand, neutron-star matter is charge-neutral before the merger, consisting mainly of neutrons with a small admixture of protons and electrons in beta-equilibrium, i.e., $[-0.5 \lesssim Y_{\text{iso}} \lesssim 0.4]$. These differences only slightly affect the region at high densities where the crossing appears in the CMF model (see, e.g., [6, 97–99] for a more detailed discussion).

The entire evolution of these systems in the QCD phase diagram is presented in Fig. 3, which shows the spatial and tem-

poral evolution in temperature and density of the various fluid cells. This is obtained by binning, across the whole evolution and for both BNS mergers and HICs, all fluid elements according to their temperature and density. As a simplification, for BNS mergers we assume the equatorial plane dynamics to be representative of the overall dynamics, thus performing a $2 + 1$ binning; for the HIC, the full $3 + 1$ dynamics is used. For BNSs, we show the results of two distinct merger simulations differing in their total respective masses, namely, for a binary with $M_{\text{tot}} = 2.6 M_{\odot}$ (top left panel) and $2.8 M_{\odot}$ (bottom left panel), respectively. For HICs, instead, we show the results at two different beam (kinetic) energies, namely at $E_{\text{lab}} = 450 A \text{ MeV}$ (top right panel) and at $600 A \text{ MeV}$ (bottom right panel), respectively.

The left panel of Fig. 3 shows a broad range of densities, $n \lesssim 3.4 n_{\text{sat}}$ and temperatures, $T \lesssim 40 \text{ MeV}$ covered by BNS mergers. Two distinct regions appear in the phase diagram during and after the merger: the first is at large densities, $n > 2 n_{\text{sat}}$, and small temperatures, $T \lesssim 10 \text{ MeV}$. This region corresponds to the central regions of the initial stars and the core of the post-merger remnant. As we have seen in Fig. 2, the neutron-star matter in this region does not undergo shock heating, but remains cold and at small entropies. Indeed, the oscillations seen at the lowest temperatures correspond to quadrupolar post-merger oscillations of the gravitationally bound rotating remnant [100]. This underlines the fact, that the behavior of this region is governed by strong gravity and, hence, has no counterpart in HICs. The second region spanned by BNS mergers in the phase diagram corresponds, instead, to hot matter with $T \gtrsim 10 \text{ MeV}$ and isentropes of $S/A = [1.8, 2.2]$, which were previously identified with the hot ring in the discussion of collision-shock dynamics (Fig. 2). We point out that the phase-diagram distributions shown in Fig. 3 for the two binaries considered (top and bottom left panels of Fig. 3), clearly exhibit that the smaller-mass binary populates regions with smaller densities and temperatures ($n \lesssim n_{\text{sat}}$, $T \lesssim 10 \text{ MeV}$), which are essentially void in the case of the high-mass binary (see dark region around $n \sim \frac{1}{2} n_{\text{sat}}$). On the other hand, small-density, high-temperature regions ($n \lesssim n_{\text{sat}}$, $T \lesssim 30 \text{ MeV}$) are richly populated for the case of the high-mass binary (see bright region around $n \lesssim 0.2 n_{\text{sat}}$). Interestingly, for both BNS masses, similar isentropes of $S/A \approx 2$ are populated. This range of entropies can be considered as characteristic for the hot matter probed in BNSs mergers and low-energy HICs. Finally, because in the CMF model adopted here a significant quark fraction can only build up in the CMF model at densities $n_b \gtrsim 3 n_{\text{sat}}$ for the low temperatures reached in both BNSs and HICs, $T \lesssim 80 \text{ MeV}$, and since the hot/high entropy matter formed in BNSs only reach densities up to $n \approx 2 n_{\text{sat}}$, no deconfined matter is expected to be produced in these simulations. In spite of that, a myriad of exotic baryons and mesons predicted by QCD are produced.

In full analogy, the right panels of Fig. 3 show the population in the phase diagrams in the case of two HICs whose beam energies have been selected so as to provide a distri-

bution in phase comparable to that of a BNS merger, namely, $E_{\text{lab}} = 450 A \text{ MeV}$ and $600 A \text{ MeV}$, respectively. Differently from the BNS merger, the expansion of the HIC remnant after the initial collision leads to an almost isentropic expansion that populates the isentropes at $S/A \sim 2$. Clearly, different beam energies populate isentropes at lower/larger values of S/A (top/bottom panels of Fig. 3). The rapid expansion from right to left along the isentrope continues until matter becomes too dilute to maintain local equilibrium and freezes out at $n \approx \frac{1}{2} n_{\text{sat}}$.

A particularly important result of this work – and clearly represented in Fig. 3 – the use of $S/A = [1.8, 2.2]$ isentropes to construct a mapping between gravitational masses of BNSs, i.e., $M_{\text{tot}} = 2.6 - 2.8 M_{\odot}$, and the beam energies of heavy-ion experiments conducted in laboratories, i.e., $E_{\text{lab}} = [450, 600] A \text{ MeV}$ [101]. To the best of our knowledge, this is the first quantitative bridging across 18 orders of magnitude between microscopic ion collisions and macroscopic astrophysical compact objects.

ACKNOWLEDGEMENTS

The authors thank M. Alford, T. Galatyuk, J. Noronha-Hostler, and C. Raithel for insightful discussions and comments. ERM gratefully acknowledges support from postdoctoral fellowships at the Princeton Center for Theoretical Science, the Princeton Gravity Initiative, and the Institute for Advanced Study. AM acknowledges the Stern-Gerlach Postdoctoral fellowship of the Stiftung Polytechnische Gesellschaft. JS thank the Samson AG and the BMBF through the ErUM-Data project for funding. VD acknowledges support from the National Science Foundation under grants PHY1748621, NP3M PHY-2116686, and MUSES OAC-2103680. LR acknowledges funding by the State of Hesse within the Research Cluster ELEMENTS (Project ID 500/10.006), by the ERC Advanced Grant “JETSET: Launching, propagation and emission of relativistic jets from binary mergers and across mass scales” (Grant No. 884631), and by HGS-HIRE for FAIR. HS acknowledges the Walter Greiner Gesellschaft zur Förderung der physikalischen Grundlagenforschung e.V. through the Judah M. Eisenberg Laureatus Chair at Goethe Universität.

-
- [1] B. P. Abbott *et al.* (LIGO Scientific, Virgo), GW170817: Observation of Gravitational Waves from a Binary Neutron Star Inspiral, *Phys. Rev. Lett.* **119**, 161101 (2017), [arXiv:1710.05832 \[gr-qc\]](https://arxiv.org/abs/1710.05832).
 - [2] B. P. Abbott *et al.* (LIGO Scientific, Virgo), GW190425: Observation of a Compact Binary Coalescence with Total Mass $\sim 3.4 M_{\odot}$, *Astrophys. J. Lett.* **892**, L3 (2020), [arXiv:2001.01761 \[astro-ph.HE\]](https://arxiv.org/abs/2001.01761).
 - [3] R. Oechslin, K. Uryu, G. S. Poghosyan, and F. K. Thielemann, The Influence of quark matter at high densities on binary neutron star mergers, *Mon. Not. Roy. Astron. Soc.* **349**, 1469 (2004), [arXiv:astro-ph/0401083](https://arxiv.org/abs/astro-ph/0401083).

- [4] E. R. Most, L. J. Papenfort, V. Dexheimer, M. Hanauske, S. Schramm, H. Stöcker, and L. Rezzolla, Signatures of quark-hadron phase transitions in general-relativistic neutron-star mergers, *Phys. Rev. Lett.* **122**, 061101 (2019), [arXiv:1807.03684 \[astro-ph.HE\]](#).
- [5] A. Bauswein, N.-U. F. Bastian, D. B. Blaschke, K. Chatziioannou, J. A. Clark, T. Fischer, and M. Oertel, Identifying a first-order phase transition in neutron star mergers through gravitational waves, *Phys. Rev. Lett.* **122**, 061102 (2019), [arXiv:1809.01116 \[astro-ph.HE\]](#).
- [6] E. R. Most, L. Jens Papenfort, V. Dexheimer, M. Hanauske, H. Stoecker, and L. Rezzolla, On the deconfinement phase transition in neutron-star mergers, *Eur. Phys. J. A* **56**, 59 (2020), [arXiv:1910.13893 \[astro-ph.HE\]](#).
- [7] M. Hanauske, J. Steinheimer, A. Motornenko, V. Vovchenko, L. Bovard, E. R. Most, L. J. Papenfort, S. Schramm, and H. Stöcker, Neutron Star Mergers: Probing the EoS of Hot, Dense Matter by Gravitational Waves, *Particles* **2**, 44 (2019).
- [8] L. R. Weih, M. Hanauske, and L. Rezzolla, Postmerger Gravitational-Wave Signatures of Phase Transitions in Binary Mergers, *Phys. Rev. Lett.* **124**, 171103 (2020), [arXiv:1912.09340 \[gr-qc\]](#).
- [9] R. Kashyap *et al.*, Numerical relativity simulations of prompt collapse mergers: threshold mass and phenomenological constraints on neutron star properties after GW170817 (2021), [arXiv:2111.05183 \[astro-ph.HE\]](#).
- [10] M. Hanauske, J. Steinheimer, L. Bovard, A. Mukherjee, S. Schramm, K. Takami, J. Papenfort, N. Wechselberger, L. Rezzolla, and H. Stöcker, Concluding Remarks: Connecting Relativistic Heavy Ion Collisions and Neutron Star Mergers by the Equation of State of Dense Hadron- and Quark Matter as signalled by Gravitational Waves, *J. Phys. Conf. Ser.* **878**, 012031 (2017).
- [11] J. Adamczewski-Musch *et al.* (HADES), Probing dense baryon-rich matter with virtual photons, *Nature Phys.* **15**, 1040 (2019).
- [12] R. Abbott *et al.* (LIGO Scientific, Virgo), GW190814: Gravitational Waves from the Coalescence of a 23 Solar Mass Black Hole with a 2.6 Solar Mass Compact Object, *Astrophys. J. Lett.* **896**, L44 (2020), [arXiv:2006.12611 \[astro-ph.HE\]](#).
- [13] B. Margalit and B. D. Metzger, Constraining the Maximum Mass of Neutron Stars From Multi-Messenger Observations of GW170817, *Astrophys. J. Lett.* **850**, L19 (2017), [arXiv:1710.05938 \[astro-ph.HE\]](#).
- [14] L. Rezzolla, E. R. Most, and L. R. Weih, Using gravitational-wave observations and quasi-universal relations to constrain the maximum mass of neutron stars, *Astrophys. J. Lett.* **852**, L25 (2018), [arXiv:1711.00314 \[astro-ph.HE\]](#).
- [15] M. Ruiz, S. L. Shapiro, and A. Tsokaros, GW170817, General Relativistic Magnetohydrodynamic Simulations, and the Neutron Star Maximum Mass, *Phys. Rev. D* **97**, 021501 (2018), [arXiv:1711.00473 \[astro-ph.HE\]](#).
- [16] M. Shibata, E. Zhou, K. Kiuchi, and S. Fujibayashi, Constraint on the maximum mass of neutron stars using GW170817 event, *Phys. Rev. D* **100**, 023015 (2019), [arXiv:1905.03656 \[astro-ph.HE\]](#).
- [17] E. Annala, T. Gorda, A. Kurkela, and A. Vuorinen, Gravitational-wave constraints on the neutron-star-matter Equation of State, *Phys. Rev. Lett.* **120**, 172703 (2018), [arXiv:1711.02644 \[astro-ph.HE\]](#).
- [18] D. Radice, A. Perego, F. Zappa, and S. Bernuzzi, GW170817: Joint Constraint on the Neutron Star Equation of State from Multimessenger Observations, *Astrophys. J. Lett.* **852**, L29 (2018), [arXiv:1711.03647 \[astro-ph.HE\]](#).
- [19] A. Bauswein, O. Just, H.-T. Janka, and N. Stergioulas, Neutron-star radius constraints from GW170817 and future detections, *Astrophys. J. Lett.* **850**, L34 (2017), [arXiv:1710.06843 \[astro-ph.HE\]](#).
- [20] E. R. Most, L. R. Weih, L. Rezzolla, and J. Schaffner-Bielich, New constraints on radii and tidal deformabilities of neutron stars from GW170817, *Phys. Rev. Lett.* **120**, 261103 (2018), [arXiv:1803.00549 \[gr-qc\]](#).
- [21] B. P. Abbott *et al.* (LIGO Scientific, Virgo), GW170817: Measurements of neutron star radii and equation of state, *Phys. Rev. Lett.* **121**, 161101 (2018), [arXiv:1805.11581 \[gr-qc\]](#).
- [22] C. Raithel, F. Özel, and D. Psaltis, Tidal deformability from GW170817 as a direct probe of the neutron star radius, *Astrophys. J. Lett.* **857**, L23 (2018), [arXiv:1803.07687 \[astro-ph.HE\]](#).
- [23] S. De, D. Finstad, J. M. Lattimer, D. A. Brown, E. Berger, and C. M. Biwer, Tidal Deformabilities and Radii of Neutron Stars from the Observation of GW170817, *Phys. Rev. Lett.* **121**, 091102 (2018), [Erratum: *Phys.Rev.Lett.* 121, 259902 (2018)], [arXiv:1804.08583 \[astro-ph.HE\]](#).
- [24] K. Chatziioannou, C.-J. Haster, and A. Zimmerman, Measuring the neutron star tidal deformability with equation-of-state-independent relations and gravitational waves, *Phys. Rev. D* **97**, 104036 (2018), [arXiv:1804.03221 \[gr-qc\]](#).
- [25] Z. Carson, A. W. Steiner, and K. Yagi, Constraining nuclear matter parameters with GW170817, *Phys. Rev. D* **99**, 043010 (2019), [arXiv:1812.08910 \[gr-qc\]](#).
- [26] V. Dexheimer, R. de Oliveira Gomes, S. Schramm, and H. Pais, What do we learn about vector interactions from GW170817?, *J. Phys. G* **46**, 034002 (2019), [arXiv:1810.06109 \[nucl-th\]](#).
- [27] Y. Lim and J. W. Holt, Bayesian modeling of the nuclear equation of state for neutron star tidal deformabilities and GW170817, *Eur. Phys. J. A* **55**, 209 (2019), [arXiv:1902.05502 \[nucl-th\]](#).
- [28] R. Essick, P. Landry, and D. E. Holz, Nonparametric Inference of Neutron Star Composition, Equation of State, and Maximum Mass with GW170817, *Phys. Rev. D* **101**, 063007 (2020), [arXiv:1910.09740 \[astro-ph.HE\]](#).
- [29] E. R. Most, L. J. Papenfort, L. R. Weih, and L. Rezzolla, A lower bound on the maximum mass if the secondary in GW190814 was once a rapidly spinning neutron star, *Mon. Not. Roy. Astron. Soc.* **499**, L82 (2020), [arXiv:2006.14601 \[astro-ph.HE\]](#).
- [30] H. Tan, J. Noronha-Hostler, and N. Yunes, Neutron Star Equation of State in light of GW190814, *Phys. Rev. Lett.* **125**, 261104 (2020), [arXiv:2006.16296 \[astro-ph.HE\]](#).
- [31] H. Tan, T. Dore, V. Dexheimer, J. Noronha-Hostler, and N. Yunes, Extreme matter meets extreme gravity: Ultraheavy neutron stars with phase transitions, *Phys. Rev. D* **105**, 023018 (2022), [arXiv:2106.03890 \[astro-ph.HE\]](#).
- [32] H. Tan, V. Dexheimer, J. Noronha-Hostler, and N. Yunes, The slope, the hill, the drop, and the swoosh: Learning about the nuclear matter equation of state from the binary Love relations (2021), [arXiv:2111.10260 \[astro-ph.HE\]](#).
- [33] A. Nathanail, E. R. Most, and L. Rezzolla, GW170817 and GW190814: tension on the maximum mass, *Astrophys. J. Lett.* **908**, L28 (2021), [arXiv:2101.01735 \[astro-ph.HE\]](#).
- [34] G. Raaijmakers, S. K. Greif, K. Hebeler, T. Hinderer, S. Nisanke, A. Schwenk, T. E. Riley, A. L. Watts, J. M. Lattimer, and W. C. G. Ho, Constraints on the Dense Matter Equation of State and Neutron Star Properties from NICER's Mass-Radius Estimate of PSR J0740+6620 and Multimessenger Observations, *Astrophys. J. Lett.* **918**, L29 (2021),

- arXiv:2105.06981 [astro-ph.HE].
- [35] M. C. Miller *et al.*, The Radius of PSR J0740+6620 from NICER and XMM-Newton Data, *Astrophys. J. Lett.* **918**, L28 (2021), arXiv:2105.06979 [astro-ph.HE].
- [36] M. Fasano, T. Abdelsalhin, A. Maselli, and V. Ferrari, Constraining the Neutron Star Equation of State Using Multiband Independent Measurements of Radii and Tidal Deformabilities, *Phys. Rev. Lett.* **123**, 141101 (2019), arXiv:1902.05078 [astro-ph.HE].
- [37] A. Bauswein, N.-U. Friedrich Bastian, D. Blaschke, K. Chatziioannou, J. A. Clark, T. Fischer, H.-T. Janka, O. Just, M. Oertel, and N. Stergioulas, Equation-of-state Constraints and the QCD Phase Transition in the Era of Gravitational-Wave Astronomy, *AIP Conf. Proc.* **2127**, 020013 (2019), arXiv:1904.01306 [astro-ph.HE].
- [38] C. D. Capano, I. Tews, S. M. Brown, B. Margalit, S. De, S. Kumar, D. A. Brown, B. Krishnan, and S. Reddy, Stringent constraints on neutron-star radii from multimessenger observations and nuclear theory, *Nature Astron.* **4**, 625 (2020), arXiv:1908.10352 [astro-ph.HE].
- [39] T. Dietrich, M. W. Coughlin, P. T. H. Pang, M. Bulla, J. Heinzel, L. Issa, I. Tews, and S. Antier, Multimessenger constraints on the neutron-star equation of state and the Hubble constant, *Science* **370**, 1450 (2020), arXiv:2002.11355 [astro-ph.HE].
- [40] P. Landry, R. Essick, and K. Chatziioannou, Nonparametric constraints on neutron star matter with existing and upcoming gravitational wave and pulsar observations, *Phys. Rev. D* **101**, 123007 (2020), arXiv:2003.04880 [astro-ph.HE].
- [41] M. Al-Mamun, A. W. Steiner, J. Nättilä, J. Lange, R. O’Shaughnessy, I. Tews, S. Gandolfi, C. Heinke, and S. Han, Combining Electromagnetic and Gravitational-Wave Constraints on Neutron-Star Masses and Radii, *Phys. Rev. Lett.* **126**, 061101 (2021), arXiv:2008.12817 [astro-ph.HE].
- [42] Y. Zhou, L.-W. Chen, and Z. Zhang, Equation of state of dense matter in the multimessenger era, *Phys. Rev. D* **99**, 121301 (2019), arXiv:1901.11364 [nucl-th].
- [43] N.-B. Zhang, B.-A. Li, and J. Xu, Combined Constraints on the Equation of State of Dense Neutron-rich Matter from Terrestrial Nuclear Experiments and Observations of Neutron Stars, *Astrophys. J.* **859**, 90 (2018), arXiv:1801.06855 [nucl-th].
- [44] P. G. Krastev and B.-A. Li, Imprints of the nuclear symmetry energy on the tidal deformability of neutron stars, *J. Phys. G* **46**, 074001 (2019), arXiv:1801.04620 [nucl-th].
- [45] B. T. Reed, F. J. Fattoyev, C. J. Horowitz, and J. Piekarewicz, Implications of PREX-2 on the Equation of State of Neutron-Rich Matter, *Phys. Rev. Lett.* **126**, 172503 (2021), arXiv:2101.03193 [nucl-th].
- [46] C. Y. Tsang, M. B. Tsang, P. Danielewicz, W. G. Lynch, and F. J. Fattoyev, Towards a better understanding of the symmetry energy within neutron stars (2019), arXiv:1901.07673 [nucl-ex].
- [47] B. Kumar, Neutron skins of heavy nuclei and tidal deformability of neutron star, *JPS Conf. Proc.* **31**, 011052 (2020), arXiv:1908.02909 [nucl-th].
- [48] V. Sagun, I. Lopes, and A. Ivanytskyi, Neutron stars meet constraints from high and low energy nuclear physics, *Nucl. Phys. A* **982**, 883 (2019), arXiv:1810.04245 [astro-ph.HE].
- [49] B.-A. Li and W.-J. Xie, Symmetry energy of super-dense neutron-rich matter from integrating barotropic pressures in neutron stars and heavy-ion reactions, *Phys. Lett. B* **806**, 135517 (2020), arXiv:1909.06616 [nucl-th].
- [50] J. J. Li, A. Sedrakian, and M. Alford, Relativistic hybrid stars in the light of NICER PSR J0740+6620 radius measurement (2021), arXiv:2108.13071 [astro-ph.HE].
- [51] B. Biswas, Impact of PREX-II and Combined Radio/NICER/XMM-Newton’s Mass–radius Measurement of PSR J0740+6620 on the Dense-matter Equation of State, *Astrophys. J.* **921**, 63 (2021), arXiv:2105.02886 [astro-ph.HE].
- [52] S. Huth *et al.*, Constraining Neutron-Star Matter with Microscopic and Macroscopic Collisions (2021), arXiv:2107.06229 [nucl-th].
- [53] S. K. Biswal, H. C. Das, A. Kumar, and S. K. Patra, Constraining nuclear matter parameters and neutron star observables using PREX-2 and NICER data (2021), arXiv:2109.11895 [nucl-th].
- [54] C. Drischler, S. Han, and S. Reddy, Large and massive neutron stars: Implications for the sound speed in dense QCD (2021), arXiv:2110.14896 [nucl-th].
- [55] M. Ferreira and C. Providência, Constraints on high density equation of state from maximum neutron star mass, *Phys. Rev. D* **104**, 063006 (2021), arXiv:2110.00305 [nucl-th].
- [56] S. Borsanyi, Z. Fodor, C. Hoelbling, S. D. Katz, S. Krieg, and K. K. Szabo, Full result for the QCD equation of state with 2+1 flavors, *Phys. Lett. B* **730**, 99 (2014), arXiv:1309.5258 [hep-lat].
- [57] A. Bazavov *et al.* (HotQCD), Equation of state in (2+1)-flavor QCD, *Phys. Rev. D* **90**, 094503 (2014), arXiv:1407.6387 [hep-lat].
- [58] A. Bazavov *et al.*, The QCD Equation of State to $\mathcal{O}(\mu_B^6)$ from Lattice QCD, *Phys. Rev. D* **95**, 054504 (2017), arXiv:1701.04325 [hep-lat].
- [59] E. S. Fraga, A. Kurkela, and A. Vuorinen, Interacting quark matter equation of state for compact stars, *Astrophys. J. Lett.* **781**, L25 (2014), arXiv:1311.5154 [nucl-th].
- [60] N. Haque, A. Bandyopadhyay, J. O. Andersen, M. G. Mustafa, M. Strickland, and N. Su, Three-loop HTLpt thermodynamics at finite temperature and chemical potential, *JHEP* **05**, 027 (2014), arXiv:1402.6907 [hep-ph].
- [61] S. Pratt, E. Sangaline, P. Sorensen, and H. Wang, Constraining the Eq. of State of Super-Hadronic Matter from Heavy-Ion Collisions, *Phys. Rev. Lett.* **114**, 202301 (2015), arXiv:1501.04042 [nucl-th].
- [62] P. Papazoglou, D. Zschesche, S. Schramm, J. Schaffner-Bielich, H. Stoecker, and W. Greiner, Nuclei in a chiral SU(3) model, *Phys. Rev. C* **59**, 411 (1999), arXiv:nucl-th/9806087.
- [63] V. Dexheimer and S. Schramm, Proto-Neutron and Neutron Stars in a Chiral SU(3) Model, *Astrophys. J.* **683**, 943 (2008), arXiv:0802.1999 [astro-ph].
- [64] A. Motornenko, J. Steinheimer, V. Vovchenko, S. Schramm, and H. Stoecker, Equation of state for hot QCD and compact stars from a mean field approach, *Phys. Rev. C* **101**, 034904 (2020), arXiv:1905.00866 [hep-ph].
- [65] P. Zyla *et al.* (Particle Data Group), Review of Particle Physics, *PTEP* **2020**, 083C01 (2020).
- [66] J. Steinheimer, S. Schramm, and H. Stoecker, An Effective chiral Hadron-Quark Equation of State Part I: Zero baryochemical potential (2009), arXiv:0909.4421 [hep-ph].
- [67] D. H. Rischke, M. I. Gorenstein, H. Stoecker, and W. Greiner, Excluded volume effect for the nuclear matter equation of state, *Z. Phys. C* **51**, 485 (1991).
- [68] K. Fukushima, Chiral effective model with the Polyakov loop, *Phys. Lett. B* **591**, 277 (2004), arXiv:hep-ph/0310121.
- [69] C. Ratti, M. A. Thaler, and W. Weise, Phases of QCD: Lattice thermodynamics and a field theoretical model, *Phys. Rev. D*

- 73, 014019 (2006), [arXiv:hep-ph/0506234](#).
- [70] J. P. Boris and D. L. Book, Flux-corrected transport. I. SHASTA, a fluid transport algorithm that works, *J. Comput. Phys.* **11**, 38 (1973).
- [71] D. H. Rischke, S. Bernard, and J. A. Maruhn, Relativistic hydrodynamics for heavy ion collisions. 1. General aspects and expansion into vacuum, *Nucl. Phys. A* **595**, 346 (1995), [arXiv:nucl-th/9504018](#).
- [72] M. Omana Kuttan, A. Motornenko, J. Steinheimer, H. Stoecker, Y. Nara, and M. Bleicher, A Chiral Mean-Field Equation-of-State in UrQMD: Effects on the Heavy Ion Compression Stage, *arXiv e-prints*, [arXiv:2201.01622](#) (2022), [arXiv:2201.01622 \[nucl-th\]](#).
- [73] G. Inghirami and H. Elfner, The applicability of hydrodynamics in heavy ion collisions at $\sqrt{s_{NN}}=2.4-7.7$ GeV, *arXiv e-prints*, [arXiv:2201.05934](#) (2022), [arXiv:2201.05934 \[hep-ph\]](#).
- [74] L. Rezzolla and O. Zanotti, *Relativistic Hydrodynamics* (OUP Oxford, 2013).
- [75] D. Hilditch, S. Bernuzzi, M. Thierfelder, Z. Cao, W. Tichy, and B. Bruegmann, Compact binary evolutions with the Z4c formulation, *Phys. Rev. D* **88**, 084057 (2013), [arXiv:1212.2901 \[gr-qc\]](#).
- [76] S. Bernuzzi and D. Hilditch, Constraint violation in free evolution schemes: Comparing BSSNOK with a conformal decomposition of Z4, *Phys. Rev. D* **81**, 084003 (2010), [arXiv:0912.2920 \[gr-qc\]](#).
- [77] D. Alic, C. Bona-Casas, C. Bona, L. Rezzolla, and C. Palenzuela, Conformal and covariant formulation of the Z4 system with constraint-violation damping, *Phys. Rev. D* **85**, 064040 (2012), [arXiv:1106.2254 \[gr-qc\]](#).
- [78] D. Alic, W. Kastaun, and L. Rezzolla, Constraint damping of the conformal and covariant formulation of the Z4 system in simulations of binary neutron stars, *Phys. Rev. D* **88**, 064049 (2013), [arXiv:1307.7391 \[gr-qc\]](#).
- [79] Z. B. Etienne, V. Paschalidis, R. Haas, P. Mösta, and S. L. Shapiro, IllinoisGRMHD: An Open-Source, User-Friendly GRMHD Code for Dynamical Spacetimes, *Class. Quant. Grav.* **32**, 175009 (2015), [arXiv:1501.07276 \[astro-ph.HE\]](#).
- [80] E. R. Most, L. J. Papenfort, and L. Rezzolla, Beyond second-order convergence in simulations of magnetized binary neutron stars with realistic microphysics, *Mon. Not. Roy. Astron. Soc.* **490**, 3588 (2019), [arXiv:1907.10328 \[astro-ph.HE\]](#).
- [81] F. Löffler *et al.*, The Einstein Toolkit: A Community Computational Infrastructure for Relativistic Astrophysics, *Class. Quant. Grav.* **29**, 115001 (2012), [arXiv:1111.3344 \[gr-qc\]](#).
- [82] E. Schnetter, S. H. Hawley, and I. Hawke, Evolutions in 3-D numerical relativity using fixed mesh refinement, *Class. Quant. Grav.* **21**, 1465 (2004), [arXiv:gr-qc/0310042](#).
- [83] E. Gourgoulhon, P. Grandclement, K. Taniguchi, J.-A. Marck, and S. Bonazzola, Quasiequilibrium sequences of synchronized and irrotational binary neutron stars in general relativity: 1. Method and tests, *Phys. Rev. D* **63**, 064029 (2001), [arXiv:gr-qc/0007028](#).
- [84] F. S. Bemfica, M. M. Disconzi, and J. Noronha, General-Relativistic Viscous Fluid Dynamics (2020), [arXiv:2009.11388 \[gr-qc\]](#).
- [85] M. Chabanov, L. Rezzolla, and D. H. Rischke, General-relativistic hydrodynamics of non-perfect fluids: 3+1 conservative formulation and application to viscous black hole accretion, *Mon. Not. Roy. Astron. Soc.* **505**, 5910 (2021), [arXiv:2102.10419 \[gr-qc\]](#).
- [86] A. Pandya and F. Pretorius, Numerical exploration of first-order relativistic hydrodynamics, *Phys. Rev. D* **104**, 023015 (2021), [arXiv:2104.00804 \[gr-qc\]](#).
- [87] E. R. Most and J. Noronha, Dissipative magnetohydrodynamics for nonresistive relativistic plasmas: An implicit second-order flux-conservative formulation with stiff relaxation, *Phys. Rev. D* **104**, 103028 (2021).
- [88] A. Harten, P. D. Lax, and B. v. Leer, On upstream differencing and godunov-type schemes for hyperbolic conservation laws, *SIAM review* **25**, 35 (1983).
- [89] P. Romatschke and U. Romatschke, *Relativistic Fluid Dynamics In and Out of Equilibrium: And Applications to Relativistic Nuclear Collisions*, Cambridge Monographs on Mathematical Physics (Cambridge University Press, 2019).
- [90] L. Baiotti and L. Rezzolla, Binary neutron star mergers: a review of Einstein’s richest laboratory, *Rept. Prog. Phys.* **80**, 096901 (2017), [arXiv:1607.03540 \[gr-qc\]](#).
- [91] L. Baiotti, B. Giacomazzo, and L. Rezzolla, Accurate evolutions of inspiralling neutron-star binaries: prompt and delayed collapse to black hole, *Phys. Rev. D* **78**, 084033 (2008), [arXiv:0804.0594 \[gr-qc\]](#).
- [92] M. Hanauske, K. Takami, L. Bovard, L. Rezzolla, J. A. Font, F. Galeazzi, and H. Stöcker, Rotational properties of hypermassive neutron stars from binary mergers, *Phys. Rev. D* **96**, 043004 (2017), [arXiv:1611.07152 \[gr-qc\]](#).
- [93] W. Kastaun, R. Cioffi, and B. Giacomazzo, Structure of Stable Binary Neutron Star Merger Remnants: a Case Study, *Phys. Rev. D* **94**, 044060 (2016), [arXiv:1607.02186 \[astro-ph.HE\]](#).
- [94] P. Arras and N. N. Weinberg, Urca reactions during neutron star inspiral, *Mon. Not. Roy. Astron. Soc.* **486**, 1424 (2019), [arXiv:1806.04163 \[astro-ph.HE\]](#).
- [95] J. S. Read, L. Baiotti, J. D. E. Creighton, J. L. Friedman, B. Giacomazzo, K. Kyutoku, C. Markakis, L. Rezzolla, M. Shibata, and K. Taniguchi, Matter effects on binary neutron star waveforms, *Phys. Rev. D* **88**, 044042 (2013), [arXiv:1306.4065 \[gr-qc\]](#).
- [96] K. Takami, L. Rezzolla, and L. Baiotti, Spectral properties of the post-merger gravitational-wave signal from binary neutron stars, *Phys. Rev. D* **91**, 064001 (2015), [arXiv:1412.3240 \[gr-qc\]](#).
- [97] E. R. Most and C. A. Raitel, Impact of the nuclear symmetry energy on the post-merger phase of a binary neutron star coalescence (2021), [arXiv:2107.06804 \[astro-ph.HE\]](#).
- [98] P. Hammond, I. Hawke, and N. Andersson, Thermal aspects of neutron star mergers, *Phys. Rev. D* **104**, 103006 (2021), [arXiv:2108.08649 \[astro-ph.HE\]](#).
- [99] A. Perego, S. Bernuzzi, and D. Radice, Thermodynamics conditions of matter in neutron star mergers, *Eur. Phys. J. A* **55**, 124 (2019), [arXiv:1903.07898 \[gr-qc\]](#).
- [100] L. Rezzolla and K. Takami, Gravitational-wave signal from binary neutron stars: a systematic analysis of the spectral properties, *Phys. Rev. D* **93**, 124051 (2016), [arXiv:1604.00246 \[gr-qc\]](#).
- [101] T. Ablyazimov *et al.* (CBM), Challenges in QCD matter physics –The scientific programme of the Compressed Baryonic Matter experiment at FAIR, *Eur. Phys. J. A* **53**, 60 (2017), [arXiv:1607.01487 \[nucl-ex\]](#).